Exp Fluids (2007) 42:659–669
DOI 10.1007/s00348-007-0270-x

RESEARCH ARTICLE

The vortex structure behind an Ahmed reference model in the presence of a moving ground plane

R. K. Strachan · K. Knowles · N. J. Lawson

Received: 2 December 2005 / Revised: 30 January 2007 / Accepted: 30 January 2007 / Published online: 28 February 2007

Abstract Laser Doppler anemometry (LDA) data are presented for an Ahmed reference model employing various backlight angles. LDA velocity measurements are taken in a number of planes around and downstream of the model at a free-stream velocity of 25 m s^{-1}. During the testing a rolling road provided ground simulation and six-component force data were recorded. Data from these experiments are compared to previous experimental data. It is found that the inclusion of the ground simulation and the consequent supporting strut produces a reduction in the size and strength of the vortices shed from the back end of the Ahmed model when compared with previous analysis. It is further concluded this effect is primarily a result of the overhead strut, and that the rolling road has little effect on these upper vortices. In addition, vortices shed from the underside of the model, not reported in previous experimental work, are found and analysed.

List of symbols

CFD	computational fluid dynamics
LDA	laser Doppler anemometry
c	support strut chord = 0.14 m
C_D	drag coefficient
C_L	lift coefficient
L	model length = 1.044 m
Re	Reynolds number
S	frontal area of Ahmed model = 0.112032 m^2
t	support strut thickness = 0.0345 m
u_∞	free-stream velocity
u, v, w	velocity components in x, y and z directions, respectively
ν	kinematic viscosity
ρ	air density

R. K. Strachan · K. Knowles (✉)
Aeromechanical Systems Group,
Department of Aerospace, Power and Sensors,
Cranfield University, Defence Academy of the UK,
Shrivenham SN6 8LA, UK
e-mail: K.Knowles@cranfield.ac.uk

N. J. Lawson
Department of Aerospace Sciences,
Cranfield University, Cranfield,
Bedfordshire MK43 0AL, UK
e-mail: N.Lawson@cranfield.ac.uk

1 Introduction

The Ahmed reference model was originally developed for a time-averaged vehicle wake investigation (Ahmed et al. 1984). It is a car-like bluff body with a curved fore body, straight centre section and an angled rear end, representing a highly simplified one-fourth-scale, lower-medium-size hatchback vehicle. The specific angle of the back end can be altered between 0° and 40°, in 5° increments. The model's major dimensions are 1044 × 389 × 288 mm. A diagram of the Ahmed reference model is shown in Fig. 1.

The Ahmed body was designed to have a fully attached flow over the front, and to exhibit many of the flow features of an automobile with its nine interchangeable rear ends. This variation in backlight geometry provides a range of flow characteristics over the back end of the model.

The geometry of this bluff body was designed to be such that an experiment could be conducted with reference to only one significant aerodynamic feature, namely the flow over the slanted rear end, as flow was expected to remain attached over the other sections. The Ahmed model has also lent itself well to the validation of CFD codes, as the

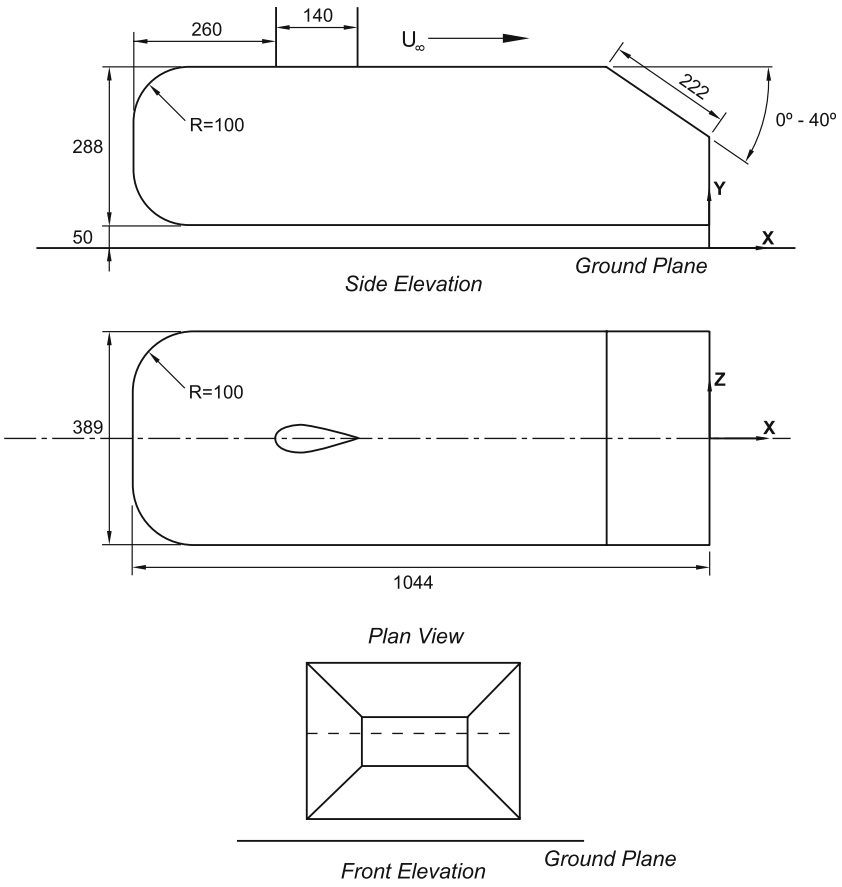

Fig. 1 Schematic diagram of Ahmed reference model (dimensions in millimetres). The flow direction and co-ordinate system used for the present study are shown

accuracy of these codes can be determined once again with only one significant aerodynamic factor varying between cases. This allows validation to be conducted without the common difficulty of sources of errors from different regions of the flow field cancelling each other out. Numerous previous experimental investigations have been reported on this model (Ahmed et al. 1984; Graysmith et al. 1994; Aider et al. 2000; Lienhart and Becker 2000, 2003; Strachan et al. 2004). These were conducted in various wind tunnels over a range of airspeeds. In general the model was supported during testing from underneath by four cylindrical struts attached to a fixed ground plane. The present tests were, however, conducted both with and without a moving ground plane with the model being supported from above by an aerodynamic strut. From the present experiments the flow regime over the Ahmed body for all nine possible back-end geometries has been recorded.

It has been shown that the flow over the angled back section is dependent on the specific backlight angle being investigated (Ahmed et al. 1984). There have been found to be two critical angles, at which the flow structure changes significantly (Gillieron and Chometon 1999). Below 12.5° (first critical angle) airflow over the angled back end remains fully attached before separating from the model when it reaches the vertical back-end. The flow from the angled section and the side walls produces a pair of counter-rotating vortices, which continue down-stream. For backlight angles between 12.5° and 30° (second critical angle) the flow over the angled section becomes highly three-dimensional. Two counter-rotating lateral vortices are again shed from the sides of the angled back section, but are larger than were formed below 12.5°. This increased vortex size affects the flow over the whole backlight, causing the three-dimensional flow. These vortices are also responsible for maintaining attached flow over a section of the backlight up to an angle of 30°, and have been shown to extend more than 500 mm (0.48 L) beyond the model trailing edge. Close to the second critical angle a separation bubble is formed over the backlight. The flow separates from the body, but re-attaches before reaching the vertical back section. At this point, the flow again separates from the model. Above 30°, flow over the angled section is fully separated. There remains though a weak tendency of the flow to turn around the side edge of the model, a result of the relative separation positions of the flow over model top and that over the backlight side edges. When the flow is in this state a near constant pressure is found across the backlight.

The current work will add to existing knowledge of the Ahmed model wake flow by analysis of LDA velocity data with the inclusion of an overhead supporting strut and both with and without a moving ground plane. In addition, the vortices shed from between the floor and side walls of the Ahmed model are analysed, as these have not previously been the subject of significant experimental study.

2 Experiments and techniques

2.1 Experimental set-up

The model was mounted 50 mm (z/L = 0.048) above a moving ground plane and supported from above by an aerodynamic strut (t/c = 0.25, positioned at 0.25 L downstream of the leading edge). This configuration allowed analysis of the effect of both the overhead strut and the moving ground plane on the flow around the model. In addition, the flow on the underside of the model and in particular the formation of any lower trailing vortices could be analysed, as their structure would not be altered by supporting struts underneath. In order to isolate the effects of both the strut and the road, tests were also repeated with a stationary ground plane.

Measurements of lift, drag and pitching moment were taken using an internal load cell mounted inside the model. Direct comparison with experimental force results from Graysmith et al. (1994) was possible owing to the similar model and strut configurations employed.

Previous LDA results on the 25° and 35° Ahmed models were made by Lienhart et al. (2002). These experiments employed four cylindrical struts to support the model from underneath and as such had no moving ground simulation. The data from these experiments will also be compared with the current data in order to ascertain what effect these differences in experimental technique may have.

2.2 Wind tunnel

The model was tested in the ''D. S. Houghton'' open-jet, closed-return wind tunnel at Shrivenham. This has nozzle dimensions of 2.74 m wide by 1.66 m high. A continuous belt rolling road (1 m wide by 3.5 m long) provided moving ground simulation. Throughout the testing the free-stream velocity was constant at 25 m s^{-1}, corresponding to a Reynolds number of approximately $Re = 1.7 \times 10^6$ (based on the model length). The rolling road was synchronised with the tunnel free-stream velocity and boundary layer control was provided by upstream suction and a knife-edge transition. The system achieved an onset boundary layer thickness of 1 mm (to 99% free-stream dynamic pressure) and a free-stream turbulence intensity below 0.25%.

2.3 Laser Doppler anemometry configuration

A two-component laser Doppler anemometer was installed on a three-dimensional computer-controlled traversing system. The 2D-LDA system consisted of DANTEC FibreFlow optics with two BSA Enhanced signal processors, Burstware software and a 2.5 m focal length DANTEC FibreFlow probe. A JEM Hydrosonic 2000 fog generator was used to seed the flow with a water/glycerol seeding mixture. Using previous error analysis, LDA velocity measurement error is predicted to be better than 1% of full-scale measurement (Lawson and Davidson 1999).

Time-averaged LDA measurements were made for the u and v components in a number of planes both around and downstream of the model. These included transverse planes at 80 mm (0.076 L), 500 mm (0.48 L) and 1044 mm (1 L) downstream and planes at the trailing edge and x = –50 mm (0.048 L) at the top of model. All back angles (0–40°) were tested, with the majority of LDA results taken from the 25° case. Figure 2 shows the planes taken for the

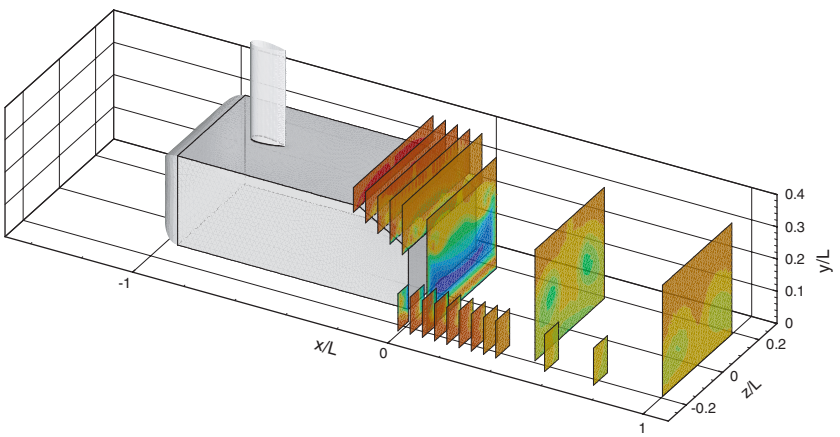

Fig. 2 LDA planes taken for 25° case

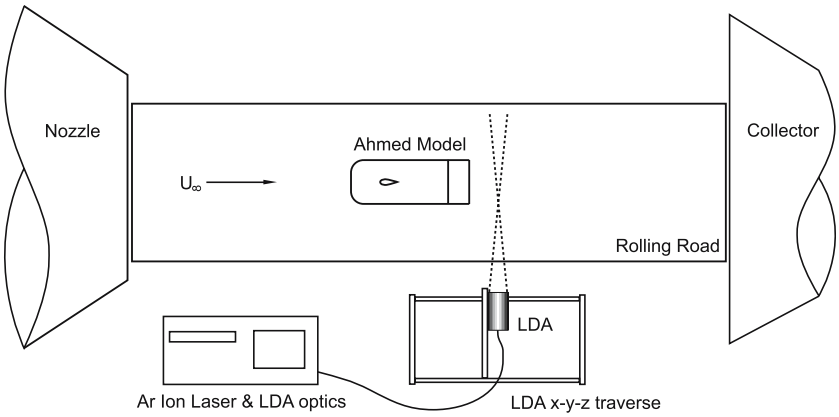

Fig. 3 Schematic diagram (plan view) of experimental set-up

25° case. Results were averaged over a 20 s sample time, with a maximum of 5000 readings being taken for both u and v velocity components at each position.

A PC-controlled six-component force balance was mounted inside the model. The force balance was calibrated with a known vertical and horizontal force prior to testing. Comparison can be made between the forces recorded and those of Graysmith et al. (1994). RMS error in force was found to be better than 1% of full-scale measurement. A schematic diagram of the experimental set-up is shown in Fig. 3.

3 Results and discussion

3.1 Comparisons with previous work

Figures 4 and 5 show the force measurements taken during the experiments compared with previously published experimental data, both with and without a moving ground plane. Lift coefficient data were not presented by Ahmed et al. (1984). It can be seen that two overall drag coefficients were recorded by Ahmed for the 30° case. These represented the high drag and low drag cases, the latter being achieved by fixing a vertical splitter plate behind the model. Graysmith et al. (1994) tested only the high drag case. For the current experiments, it appears from the results that at the critical 30° angle, interference from the overhead supporting strut may cause the separation bubble to burst between 25° and 30°. The peak in drag would therefore be expected to occur at a smaller backlight angle than in Ahmed's original experiment, causing only the low drag 30° case to be measured. The exact nature of this interference and its effect on the overall flow over the model backlight is analysed later. It is clear in all the results outlined that the trends for both lift and drag follow those expected from the flow regimes outlined earlier. The shifting of this trend—an evident increase in drag coefficient in both the investigations employing a moving ground

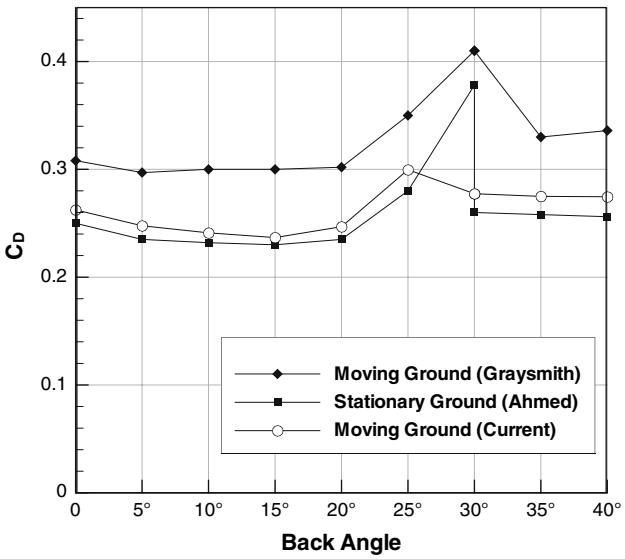

Fig. 4 Current and previous experimental C_D results for the Ahmed model

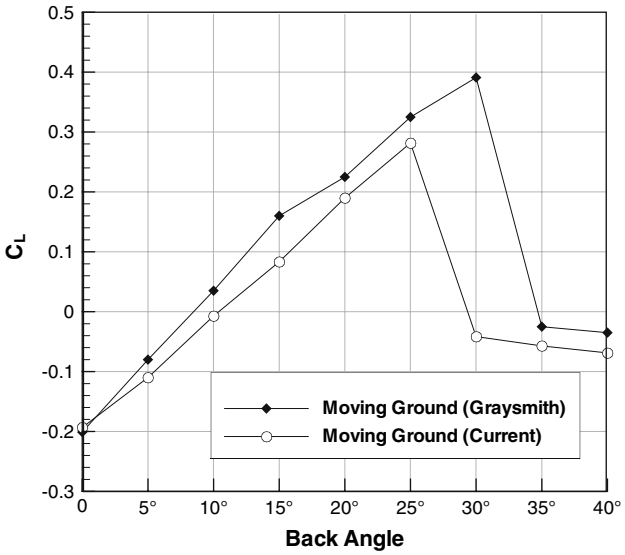

Fig. 5 Current and previous experimental C_L results for the Ahmed model

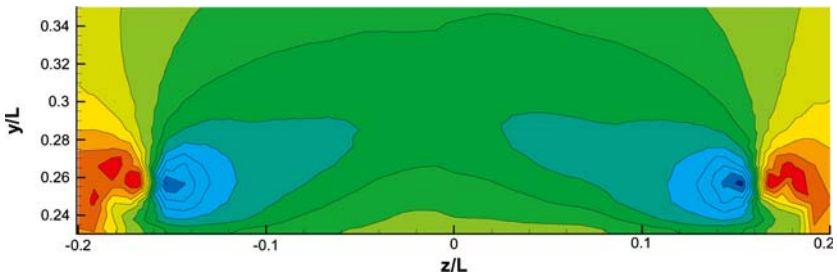

Fig. 6 v/u_∞ contour plot for 25° Ahmed model at 40 m s^{-1}, taken at the trailing edge ($x/L = 0$). LDA investigation by Lienhart et al. (2002) with fixed road

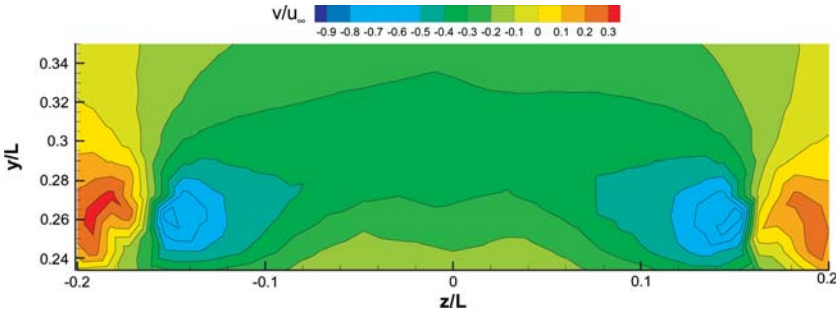

Fig. 7 v/u_∞ contour plot for 25° Ahmed model at 25 m s^{-1}, taken at the trailing edge ($x/L = 0$). Current LDA investigation with rolling road

plane—is likely to be caused by both the effect of the rolling road itself and the relocation of the supporting struts from underneath to on top of the model. The significant shift in drag coefficient between the two moving ground cases (≈15%) is, however, unexpected as they were run under very similar test conditions.

In comparing the current LDA measurements to the previous study by Lienhart et al. (2002) a number of differences between these two investigations should be noted. Lienhart et al. (2002) only tested two back angles (25° and 35°, either side of the second critical angle), whereas all back angles (0°–40°) were tested in the present work. In addition, a rolling road and overhead supporting strut were employed in the current experiments, while Lienhart et al. (2002) used a stationary ground plane with the model supported underneath by four circular struts. The measurement grid spacing used in the current study was smaller than Lienhart et al.'s (2002), which has allowed analysis of finer flow detail, notably the lower vortices created by the underside of the model. Finally, the free-stream velocity was constant at 25 m s^{-1} ($Re = 1.7 \times 10^6$) during the current experiments, whereas Lienhart et al. (2002) tested at a velocity of 40 m s^{-1} ($Re = 2.7 \times 10^6$).

Figures 6 and 7 show a comparison between these two LDA investigations, displaying a plane of data at the top end of the trailing edge for the 25° back angle. The plots are of the v velocity component non-dimensionalised with respect to the free-stream velocity. They both clearly show the two counter-rotating vortices being shed from the back end. For direct comparison a line of data has been extracted from these contour plots through the approximate centres of these vortices ($y/L = 0.26$). This is shown in Fig. 8, where the upper line represents the u velocity component with the lower representing the v component. It can be seen that the maximum positive and negative v velocities recorded by Lienhart in the vortex structure were approximately $0.1u_\infty$ higher and $0.12u_\infty$ lower, respectively, than the current experiments. This suggests the vortices shed from the trailing edge in Lienhart's tests were more energetic. Also, the velocity of the downward flow over the central section of the back end was found to be greater in the previous experiments by around $0.1u_\infty$. This increased

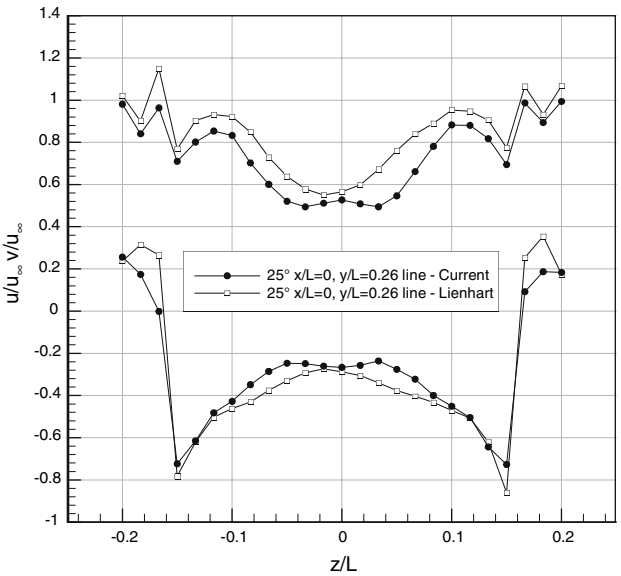

Fig. 8 Line plot of v/u_∞ and u/u_∞ for 25° Ahmed model at $y/L = 0.26$, $x/L = 0$; current and previous LDA data

downwash is consistent with the increased vortex strength. This effect is likely to be a result of increase suction caused by a higher flow velocity over the backlight in Lienhart's experiments. This is the logical result of the blockage caused by the addition of the strut in the current experiments, which will retard the flow over the top of the model and subsequently over the backlight itself. This reduced suction in the current experiments will force less flow over the sides of the backlight, resulting in the lower longitudinal vortex strength shown. There is, however, a section of the flow close to the symmetry plane of the model ($z/L = \pm 0.02$) where the current data displays a drop in the velocity of the downward flow, not found in Lienhart's data. It is thought that this may be due to the interference of the supporting strut altering the flow in this region, possibly increasing the downwash by formation of horseshoe vortices at the strut/model join.

Variation in u velocity in Fig. 8 between the two sets of results generally remains at approximately $0.1u_\infty$. This discrepancy would again be an expected result of the upstream blockage caused by the strut. Again though this is not the case between $z/L = \pm 0.02$, where the u velocity in the current experiments exhibits a rise not mirrored by Lienhart. This inconsistency is most likely a result of the strut induced downwash preventing a full development of the boundary layer over this section, in the same way that the downwash from the side vortices do over the outboard sections of the backlight.

As it is the longitudinal vortices which are responsible for maintaining attached flow up to the critical 30° angle, the less energetic vortices found in the current experiments are the expected cause of the flow separation prior to this angle in the current set-up.

Figure 9 shows further comparison between these two results. As before, a line plot of v/u_∞ through the centre of the visible vortices is shown, this time 500 mm (0.48 L) downstream of the trailing edge for the 25° case. As these vortices progress downstream they move towards the ground plane, and as such their approximate centres are now located at $y/L = 0.15$. The plots appear to follow very similar trends but with the minimum velocity magnitude recorded by Lienhart being about $0.06u_\infty$ greater than the current data. Again the increased strength of the vortices shed from the back end of Lienhart's model (shown in Fig. 8) would result in a stronger downwash.

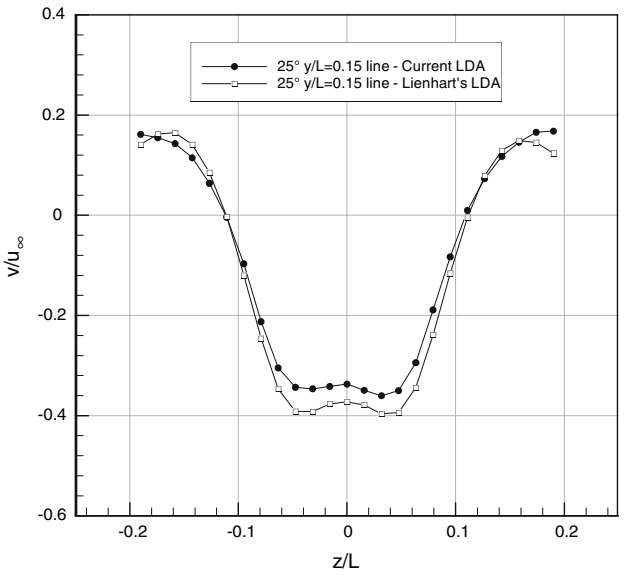

Fig. 9 Line plot of v/u_∞ for 25° Ahmed model at $y/L = 0.15$, $x/L = 0.48$; current and previous LDA data

3.2 Ground simulation effects

In order to confirm the reasoning that the strut blockage is the cause of the lower longitudinal vortex strength exhibited in the current experiments, the effect of the rolling road ground simulation, also not employed in Lienhart's experiments, must be isolated. To this end lines of data taken over the backlight at $x/L = -0.096$ and at the model trailing edge with and without ground simulation are shown in Fig. 10 and 11. Initial inspection of these figures reveals that the inclusion of the rolling road has little, if any significant effect on the strength and structure of the longitudinal vortices. Indeed the maximum and minimum recorded v velocities between the two cases at both plotted positions were found to be within $0.01u_\infty$ of each other. This in comparison to the $0.1u_\infty$ variation shown in Fig. 8. In addition, there was found to be no variation in the

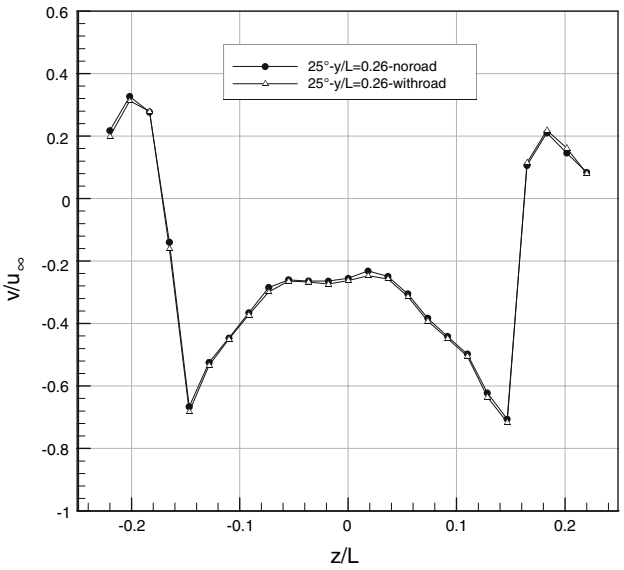

Fig. 10 Line plot of v/u_∞ for 25° Ahmed model at $y/L = 0.26$, $x/L = 0$; current LDA data with fixed and moving ground simulation

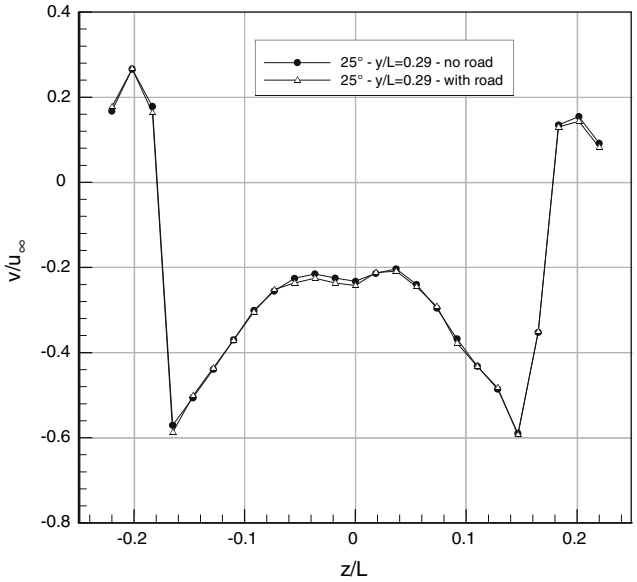

Fig. 11 Line plot of v/u_∞ for 25° Ahmed model at $y/L = 0.29$, $x/L = -0.096$; current LDA data with fixed and moving ground simulation

positions of the maxima and minima, again reinforcing the belief that it is the strut, which causes the discrepancies in longitudinal vortex formation between the current experiments and those of Lienhart et al. (2002).

3.3 Lower vortex analysis

In addition to the top longitudinal vortices observed previously over the Ahmed model backlight, the current experiments demonstrated the existence of two further vortices shed from the model underside. These were not found either in Ahmed's original experiment, or in Lienhart's results. Although the grid spacing for the LDA was finer in the current study, it would still be expected that some evidence of these lower vortices would have been found by Lienhart. As analysis of those results shows no trace, and as no report of these vortices' existence was given in Ahmed's analysis of the wake flow, it must be assumed that the inclusion of the cylindrical struts suppresses their formation. As such no direct comparison can be given with other experimental data. The position and mode of rotation of these lower vortices are shown schematically in Fig. 12, along with their larger over model counterparts. Throughout the following analysis data is presented only for the lower left vortex shown due to model symmetry.

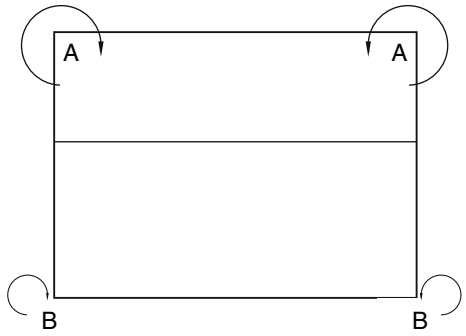

Fig. 12 Schematic diagram of positions and modes of rotation of upper and lower vortices in near-wake of Ahmed model

In order to ascertain what effect the back angle has on these lower vortices, data were taken at a number of downstream distances for both of the extreme back angle cases (0° and 40°). Figure 13 shows a comparison between these angles for a y–z plane 50 mm (0.048 L) downstream of the trailing edge.

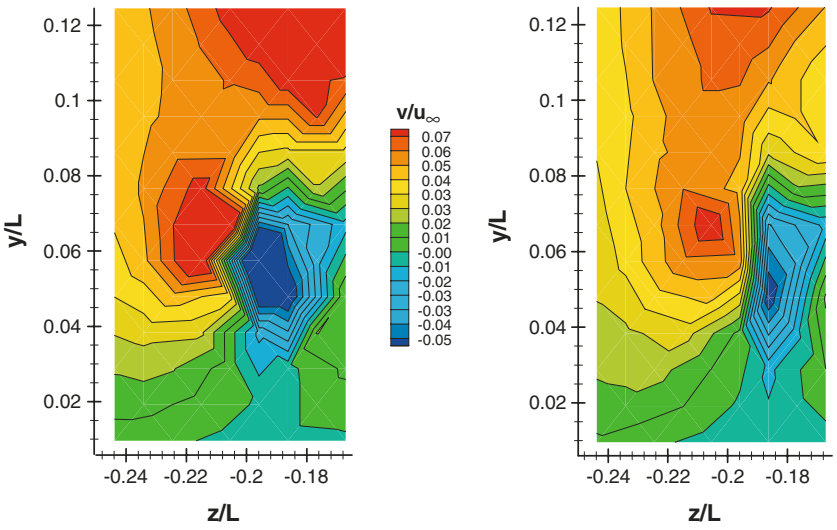

Fig. 13 v/u_∞ contour plot for 40° (*left diagram*) and 0° (*right diagram*) Ahmed models at 25 m s^{-1}, $x/L = 0.048$; current LDA investigation with rolling road

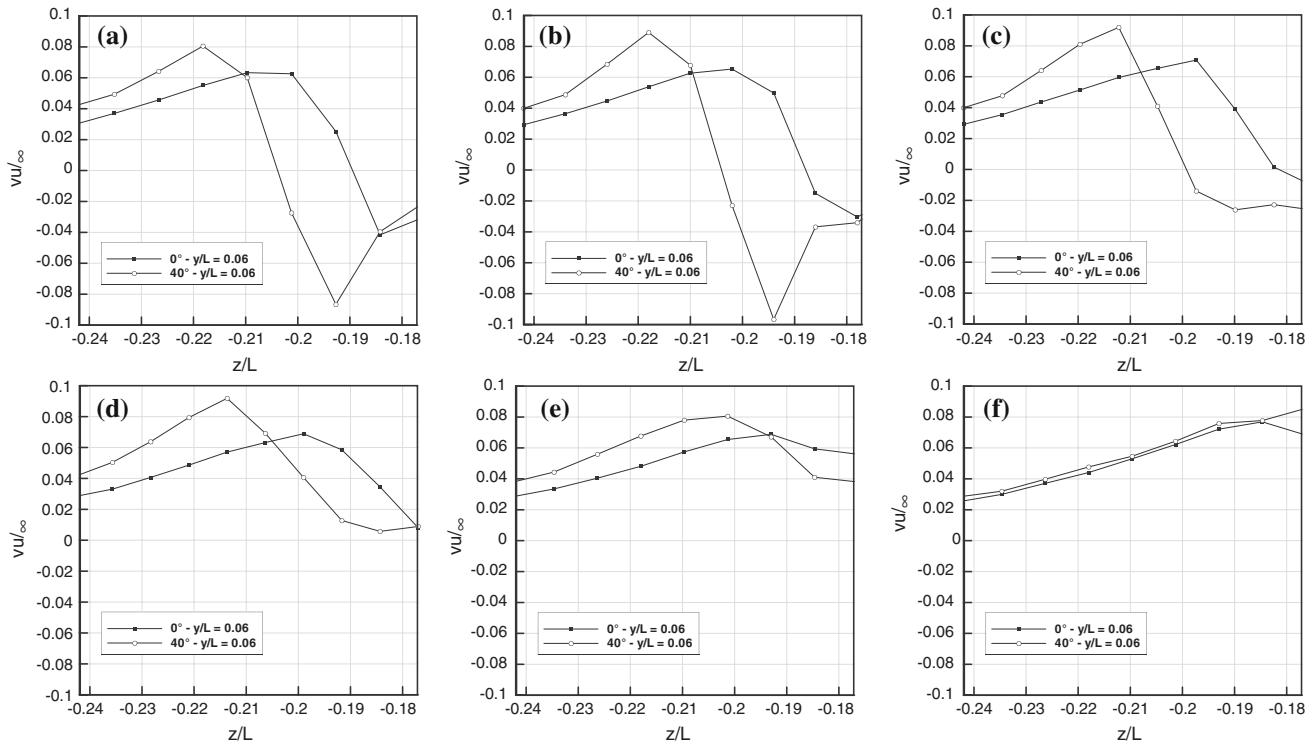

Fig. 14 Line plots of v/u_∞ for 0° and 40° Ahmed models, y/L = 0.06, x/L = 0.048–0.287; current LDA investigation with rolling road. x/L = 0.048 (**a**), 0.096 (**b**), 0.144 (**c**), 0.192 (**d**), 0.24 (**e**) and 0.287 (**f**) respectively

From Fig. 13 it is clear that both the 0° and 40° cases produce lower vortices, which are visible downstream of the trailing edge, therefore suggesting that they are produced at all intervening back angles. There is, though, a significant change in the flow structure between the first and second critical angles for which no lower vortex data have been taken, and as such further work will be required to prove that these vortices are also formed for these back angles.

It is also evident from Fig. 13 that these vortices exhibit a number of structural differences. In order that these differences can be quantified, a line of data has been extracted at a height of y/L = 0.06 for both cases, which can be seen in Fig. 14a. For the 40° case, where there is fully separated flow over the back end, the maximum negative v velocity is approximately double that of the 0° case—a difference of approximately $0.04u_\infty$. The maximum positive v velocity is also found to be greater by around $0.02u_\infty$. In addition, the centre of the vortex, identified in this case as the point where the v velocity component is zero, is found to be located at z/L = –0.204 for the 0° case, and at z/L = –0.19 for the 40° case.

It is clear, therefore, that where the flow over the trailing edge is fully separated, the lower vortex produced is both stronger and located further from the side of the model than when the flow remains fully attached. Thus, it appears that the formation of stronger trailing vortices over the top of the model in the 40° case has the effect of forcing more of the flow from the underside upwards than in the 0° case, resulting in the formation of a pair of stronger lower vortices.

Figure 14a–f show how these vortices propagate downstream of the trailing edge. At each distance downstream a line of data has been extracted at y/L = 0.06 from both 0° and 40° cases. This is at every recorded position downstream the centre of the visible vortices, as they do not appear to alter position in the y-axis.

The plots of data at 100 and 150 mm (0.095 and 0.144 L) downstream show a trailing lower vortex, with the 40° case exhibiting a more energetic vortex than its 0° counterpart (Fig. 14b, c). At 0.19 L downstream, however, both 0° and 40° plots show the vortex has already dissipated (Fig. 14d). The effects of the vortices can still be seen up to 0.24 L downstream, as shown in the plots by the line of data following the same general pattern as before (Fig. 14e), but there appears to be no vortex or spiral flow downstream of 0.14 L.

A computational investigation into the 25° Ahmed body, and employing an advanced LES turbulence model was performed by Krajnovic and Davidson (2004). In this study, the model was assumed to be sitting in mid-air,

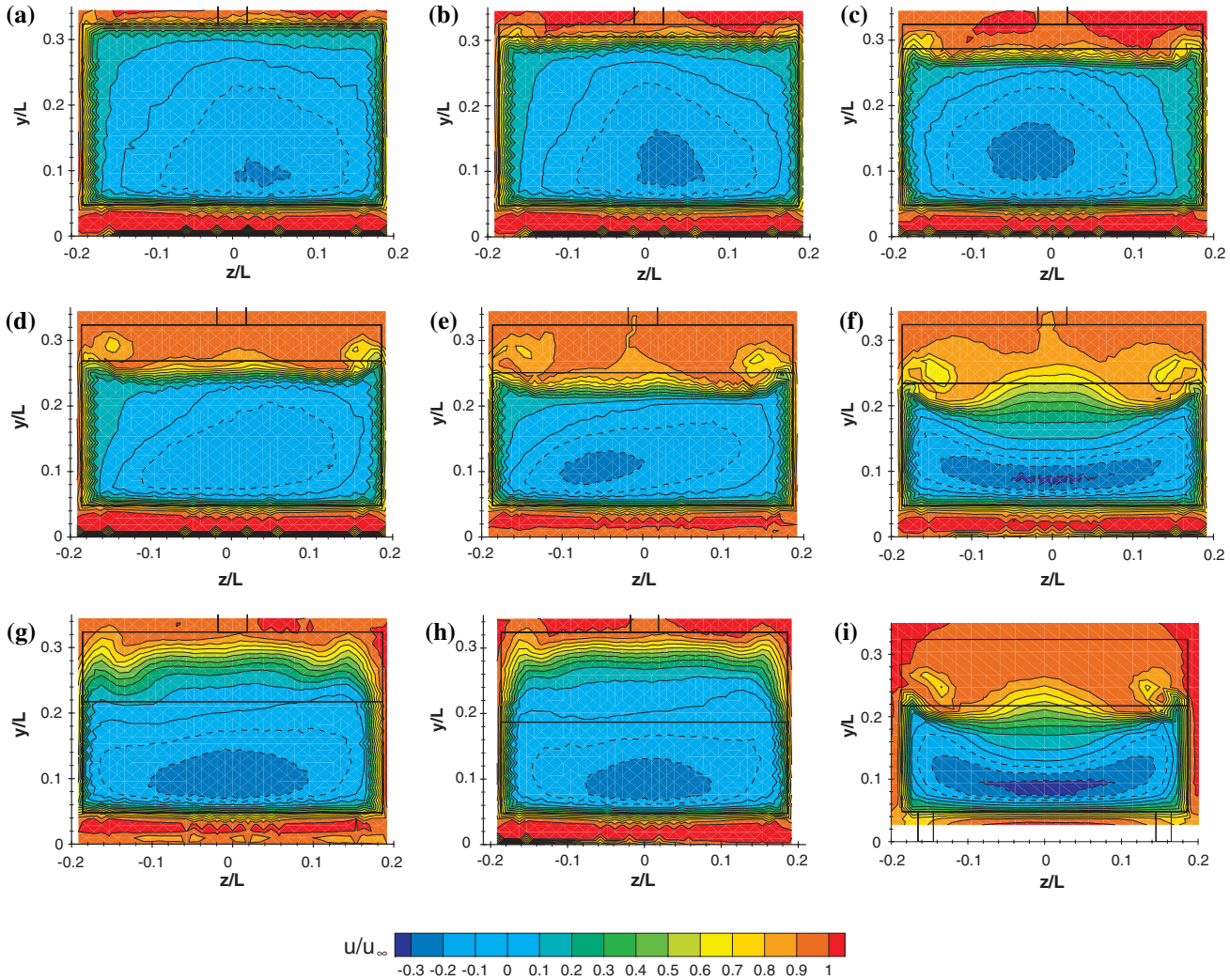

Fig. 15 Contour plots of u/u_∞ for Ahmed model at $x/L = 0.077$: current and previous LDA data. **a** 0° Ahmed models: current LDA, with rolling road; **b** 5° Ahmed models: current LDA, with rolling road; **c** 10° Ahmed models: current LDA, with rolling road; **d** 15° Ahmed model: current LDA, with rolling road; **e** 20° Ahmed model: current LDA, with rolling road; **f** 25° Ahmed model: current LDA, with rolling road; **g** 30° Ahmed model: current LDA, with rolling road; **h** 40° Ahmed model: current LDA, with rolling road; **i** 25° Ahmed model: Lienhart et al.'s (2002) LDA, with fixed road

with neither underneath or overhead struts to alter the flow. Similar lower trailing vortices were found in this case and extended from 800 mm (0.77 L) upstream to 100 mm (0.096 L) downstream of the trailing edge. Note that at the two back angles tested in the current experimental programme the lower vortices were still clearly visible at 150 mm (0.14 L) downstream, which would suggest that this may well also be the case for the intermediate angles. As such Krajnovic and Davidson's (2004) results may well under-predict the distance downstream, which these vortices travel. This may be due to the lower Reynolds number at which this computation was performed, as the stronger influence of viscous forces may be the cause of the earlier vortex breakdown.

3.4 Further LDA data analysis

Figure 15 shows contour plots of u/u_∞ for the current experiments with 0°, 5°, 10°, 15°, 20° 25°, 30° and 40° cases, in addition to Lienhart et al.'s (2002) 25° case, all at 80 mm (0.077 L) downstream of the model trailing edge. All the diagrams are plotted on the same scale with reversed flow regions bound by dashed lines, and the geometry of the model and supporting struts are also included in the plots to aid comparison. The gradual increase in the size of the vortices being shed from the top of the trailing edge between 0° and 25° can clearly be seen in Fig. 15a–f. Also the large vortices created by the 25° back angle can be seen in both the current data (Fig. 15f) and

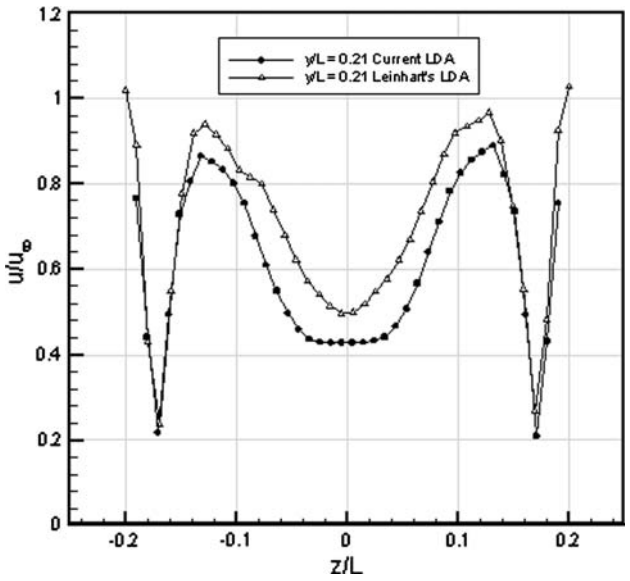

Fig. 16 Line plot of u/u_∞ for 25° Ahmed model at $y/L = 0.21$, $x/L = 0.077$; current and previous LDA data

those of Lienhart et al. (2002) (Fig. 15i). Once the back angle has increased beyond this point and the flow is fully separated over the back end, the weaker tendency of the flow to turn around the side edges of the backlight can be seen in both 30° and 40° cases.

Figure 16 shows a line plot of comparison between the current LDA results and those from Lienhart et al. (2002), taken from the data presented in Fig. 17. Plotted is u/u_∞ for the 25° case at 80 mm (0.077 L) downstream for a value of $y/L = 0.21$. Although the two plots in Fig. 16 follow virtually identical paths out with $z/L = \pm 0.15$, there is clearly a significant decrease in u/u_∞ (on average around $0.1u_\infty$) over the centre section of the back end. Is is interesting to note that this large reduction in velocity, caused by the inclusion of the supporting strut, extends to this position from the model centreline. This in comparison to the strut dimensions which extend to only $z/L = \pm 0.017$. Therefore the inclusion of the strut can be seen to alter the flow over virtually the whole backlight, resulting in the lower vortex strength outlined previously.

4 Conclusions

LDA data have been compared to previous experimental results for a number of planes both around and downstream of an Ahmed reference model.

It has been shown that the inclusion of a rolling road and the consequent overhead supporting strut has a significant effect on the flow over the back end of the Ahmed model. The overhead strut appears to reduce the strength of the counter-rotating vortices, which are formed over the top of the model, thus decreasing the downwash over the rear end. In addition, because these vortices allow the flow to remain attached until the critical angle of 30°, it is thought that this reduction in vortex strength is responsible for the separated flow observed in the current 30° test case. It has also been shown that the inclusion of the moving ground plane has little effect on the formation of these longitudinal vortices.

Lower vortices formed at the near-ground section of the model were observed during testing. These vortices had not been observed in previous, fixed ground, tests (Lienhart et al. 2002) but were simulated both by a previous computational study (Krajnovic and Davidson 2004). However, in the computational case the distance downstream, which these vortices propagate was not predicted accurately.

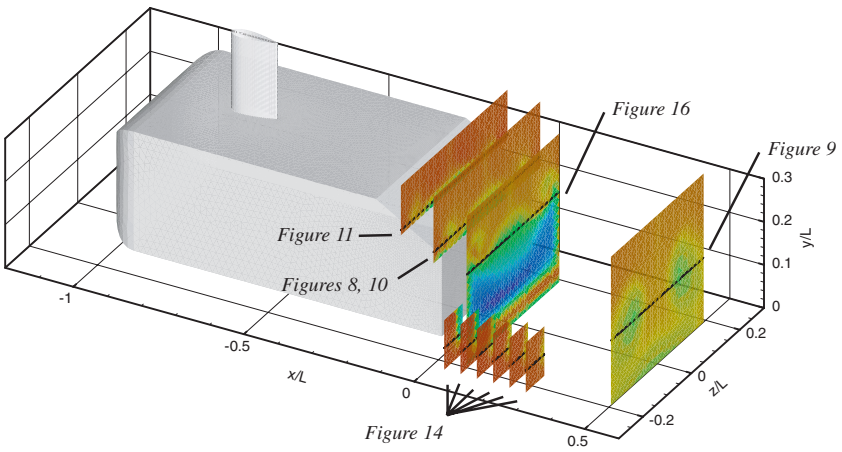

Fig. 17 Positions of data lines plotted in Figs8, 9, 10, 11, 14 and 16

References

Ahmed SR, Ramm G, Faltin G (1984) Some salient features of the time-averaged ground vehicle wake. SAE Technical Paper Series 840 300, Detroit MI

Aider JL, Dubuc L, Hulin G, Elena L (2000) Experimental and numerical investigation of the flow around a simplified vehicle shape. Third MIRA international vehicle aerodynamics conference, Rugby, UK

Gillieron P, Chometon F (1999) Modelling of stationary 3D separated air flows around an Ahmed reference model. ESAIM Proc 7:173–182

Graysmith JL, Baxendale AJ, Howell JP, Haynes T (1994) Comparisons between CFD and experimental results for the Ahmed reference model. RAeS conference on vehicle aerodynamics, Loughborough, pp 30.1–30.11

Krajnovic S, Davidson L (2004) Large-eddy simulation of the flow around simplified car model. Paper 2004-01-0227 SAE World Congress and Exhibition, Detroit

Lawson N, Davidson MR (1999) Crossflow characteristics of an oscillating jet in a thin slab casting mould. J Fluid Eng 121:588–595

Lienhart H, Becker S (2000) LDA measurements of the flow and turbulence structures in the wake of a simplified car model. Institute of Fluid Mechanics (LSTM) University Erlangen-Nuremberg

Lienhart H, Becker S (2003) Flow and turbulence structure in the wake of a simplified car model. SAE Technical Paper Series 2003-01-0656, Detroit

Lienhart H, Soots C, Becker S (2002) Flow and turbulence structures in the wake of a simplified car model (Ahmed Model). In: Proceedings DGLR Fach. Symp. der AG STAB Stuttgart University

Strachan RK, Knowles K, Lawson N. (2004) A CFD and experimental study of an Ahmed reference model. Paper 2004-01-0442 SAE World Congress and Exhibition, Detroit